J Mater Sci (2006) 41:5981–5993
DOI 10.1007/s10853-006-0254-x

Structure-property relationship in sol-gel derived polymer/silica hybrid nanocomposites prepared at various pH

Abhijit Bandyopadhyay · Mousumi De Sarkar · Anil K. Bhowmick

Received: 6 September 2004 / Accepted: 28 October 2005 / Published online: 1 August 2006

Abstract This paper reports a comparative study on structure-property relationship of acrylic rubber (ACM)/silica, epoxidised natural rubber (ENR)/silica and poly (vinyl alcohol) (PVA)/silica hybrid nanocomposites prepared by sol-gel technique under different pH levels (pH = 1.0–13.0), probably for the first time. The initial concentration of tetraethoxysilane (TEOS) (used as the precursor for silica) was kept at 45 wt%, and tetrahydrofuran (THF) for ACM/silica and ENR/silica while water for PVA/silica were taken as solvents. TEOS to water mole ratio was maintained at 1:2 for the rubber/silica systems to accomplish the sol-gel reaction. The structure of the resultant hybrid composites was determined by using electron microscopy, Fourier Transform infrared spectroscopy and solubility. Dynamic mechanical and mechanical properties were also investigated. The silica particles were found to exist as nanoparticles (average diameter < 100 nm) at low pH (≤ 2.0) beyond which these aggregate, although the amount of silica generation was not strictly influenced by the various pH conditions in all the systems. These nanocomposites were optically clear and showed superior mechanical reinforcement over the micro-composites containing aggregated silica structures with lower optical clarity. The nanocomposites exhibited higher storage modulus both at the glassy and the rubbery regions as compared to those micro-composites. The loss tangent peak heights were also minimum and the *T*g shifted to higher temperature for those nanocomposites. The maximum improvement of mechanical properties was observed with the PVA/silica nanocomposites due to higher level of interaction between the hydroxyl groups of PVA and the silanol groups of the silica phase.

A. Bandyopadhyay · M. De Sarkar · A. K. Bhowmick (✉)
Rubber Technology Centre, Indian Institute of Technology, Kharagpur 721302, India
e-mail: anilkb@rtc.iitkgp.ernet.in

Introduction

Sol-gel chemistry offers a unique advantage in the creation of novel organic–inorganic hybrids. The sol-gel process requires a combination of metal alkoxide precursors [$M(OR)_n$] and water, where M is a network forming inorganic element and R is typically an alkyl group. Hydrolysis and condensation of the metal alkoxide are the two fundamental steps to produce inorganic network within the polymer matrix in presence of an acid or base catalyst. This can be shown by the following scheme [1] (Fig. 1).

Silicon alkoxide (e.g., tetraethoxysilane, TEOS) is the most commonly used metal alkoxide due to their mild reaction condition [2, 3]. Tang and Mark [4] have reported mechanical properties of sol-gel hybrids prepared from poly (dimethyl siloxane) and TEOS. Recently the organic–inorganic hybrids have been prepared by in-situ polymerization technique [5–7], but detail investigation on structure–property relationship especially on the rubbery systems has not been reported so far. Although silica is widely used as filler in the rubber industry, literature on silica filled rubber by sol-gel technique is scanty.

The properties of the organic–inorganic hybrid composites result from the rich interplay between the constituents and are greatly influenced by the length scale of the component phases (size and shape) and

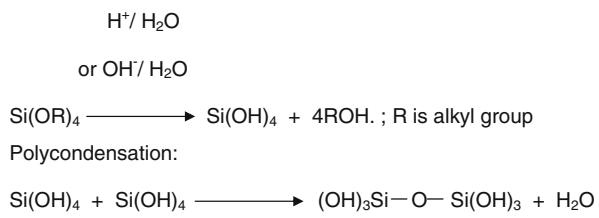

Fig. 1 Reaction scheme for the silica formation from tetraethoxysilane

also by their interfacial interaction. The reaction parameters that influence the sol-gel chemistry are the pH of the solution, the mole ratio of Si to H_2O, catalysts, solvents and reaction temperature. Also, pH plays a key role in determining the nature of the hybrids when all other parameters are kept constant. Landry et al. [8] studied the effects of pH in poly (methylmethacrylate)/silica hybrids. The hybrids formed in both acidic and basic environments show that silica uniformly disperses in the polymer matrix with particles smaller than 100 nm using an acid catalyst, while these aggregate in basic medium. In preparing polymer-inorganic hybrids, HCl is commonly used as an acid catalyst. Huang et al. [9] have observed the structure and morphology of the hybrids by using various HCl/TEOS ratios in poly (dimethyl siloxane). Nanolevel dispersion of silica particles within the hybrids in acid environment has also been reported by Zerda et al. [10] and Himmel et al. [11], but how the morphology of the silica phase affects the physical properties has not been discussed in detail.

In our earlier communication, we have reported the synthesis and characterization of various polymer/silica organic–inorganic hybrid nanocomposites by using acrylic rubber (ACM) [12], epoxidised natural rubber (ENR) [13] and poly (vinyl alcohol) (PVA) [14] with TEOS. We have also conducted a detailed study on the structure–property relationship of the rubber/silica hybrid nanocomposites (ACM and ENR based) by varying the reaction parameters like solvents, Si to H_2O mole ratio and temperature [15, 16].

Although literatures are available on sol-gel derived polymer/silica hybrid nanocomposites, comparative study describing the structure–property relationships using polymers (especially rubbers) with different interactive sites under varying pH conditions has not been reported as yet. This paper reports our results on the detailed investigation of the structure and properties of ACM/silica, ENR/silica and PVA/silica hybrid nanocomposites with the variation of pH under optimized conditions of solvent, Si to H_2O mole ratio and temperature. The present investigation offers new insight in the following aspects:

- Extent of growth of silica particles as influenced by the different pH levels and also by the polymers of different functionality, used as the matrix.
- Effect of morphology of silica particles on the physical properties of the hybrid composites.

Experimental

Materials

Poly (vinyl alcohol) (PVA, Number average degree of polymerization = 1,800, 98% hydrolyzed) was procured from Loba Chem, Mumbai, India. Epoxidised natural rubber (ENR50, with 50 mole% of epoxy content, Mooney viscosity $ML_{(1+4)}100$ °C = 140), was supplied by the Rubber Board, Kottyam, India. Henceforth, the rubber will be designated as only ENR. Acrylic rubber, ACM, Nipol AR51 (density at 25 °C = 1,100 kg/m^3, Mooney viscosity, $ML_{(1+4)}$ at 100 °C = 51) was obtained from Nippon Zeon Co. Ltd., Tokyo, Japan. It was reported to have epoxy cure site and made from ethyl acrylate monomer. Tetraethoxysilane, (TEOS, density = 930 kg/m^3, 98% pure) was procured from ACROS Organics, USA. Tetrahydrofuran, (THF, 99% pure) was purchased from Merck, Mumbai, India. Deionized water and concentrated hydrochloric acid of laboratory grade were obtained from indigenous sources.

Preparation of the hybrid composites through sol-gel technique

ACM and ENR were dissolved in THF (5% w/v), while PVA was first dissolved in boiling water (5% w/v) and then cooled to room temperature. For the rubbers, TEOS and water in the mole ratio of 1:2 along with varying proportions of concentrated HCl and for PVA, TEOS and different amounts of HCl were added to the polymer solutions under stirring conditions at room temperature (25 °C). The concentration of TEOS was fixed at 45 wt% with respect to the polymer. The samples were prepared in different acidic pH ranges (pH < 7.0) having been controlled by the addition of appropriate amount of HCl. To prepare samples under basic pH, NaOH was used as catalyst. Details of the composition of the samples are depicted in Table 1. After thorough mixing of TEOS, catalyst (HCl/NaOH) and water (for ACM and ENR) for 30 min under room temperature, the resultant solutions were cast on plane aluminium plates for gelation, till they showed practically no weight variation. The appearance of all the hybrid films is reported in Table 1. It may be

Table 1 Composition of the hybrid composites

Composite designation	pH range	Appearance of the films	Infrared optical density	Silica (wt%)[a]
ACMp1	1.0–2.0	Transparent	0.18	12.1
ACMp3	3.0–4.0	Partially opaque	0.36	12.0
ACMp5	5.0–6.0	Partially opaque	0.64	11.7
ACMp9	9.0–10.0	Partially opaque	0.60	12.2
ACMp12	12.0–13.0	Opaque	0.95	11.6
ENRp1	1.0–2.0	Transparent	0.18	11.8
ENRp3	3.0–4.0	Partially opaque	0.33	12.3
ENRp5	5.0–6.0	Partially opaque	0.48	12.1
ENRp9	9.0–10.0	Opaque	0.78	12.2
ENRp12	12.0–13.0	Opaque	0.90	12.0
PVAp1	1.0–2.0	Transparent	0.08	12.2
PVAp3	3.0–4.0	Transparent	0.10	11.8
PVAp5	5.0–6.0	Transparent	0.10	11.7
PVAp9	9.0–10.0	Transparent	0.13	12.1
PVAp12	12.0–13.0	Partially opaque	0.15	11.7

[a]The wt% silica is obtained by measuring the ash content of the hybrid composites at 800 °C for 8 h in a muffle furnace

mentioned that the relative humidity (RH) level in the air was around 90% during the testing of PVA/silica hybrid composites.

Characterization of the hybrid composite films

Transmission electron microscopy (TEM)

Transmission electron microscopic studies were performed using TEM (model C-12, Philips) on very thin films (100 nm) of the hybrid composites, cast directly over the copper grids of 300 mesh size. The acceleration voltage was 120 kV.

Scanning electron microscopy (SEM) and EDX silicon mapping

The dispersion of silica particles in the ACM matrix was observed through microscopic investigations with a JEOL JSM 5800 scanning electron microscope. The samples were sputter coated with gold in order to avoid the artifacts associated with sample charging. The acceleration voltage was 20 kV. The X-ray silicon mapping of the hybrid composite films was recorded in an Oxford EDAX system, attached to the microscope.

Infrared (IR) spectroscopy and optical density (OD)

The infrared (IR) spectra of the hybrid composite films were recorded with a Nicolet Nexus FTIR spectrophotometer in ATR mode using 45° KRS5 prism at room temperature. The samples were scanned from 4000 cm^{-1} to 600 cm^{-1} with a resolution of 4 cm^{-1}. All the spectra were taken after an average of 32 scans for each specimen. The data acquisition was done through OMNIC ESP software. The infrared optical density (OD) of the uncured composites was taken as the infrared absorbance values (A) of the composite films of average thickness 0.25 mm, which was expressed as

$$\mathrm{OD} = A = \log_{10}(I/I_0) \tag{1}$$

where I_o is the intensity of light incident on the sample and I is the reflected beam intensity. Higher the OD, lower the transmittance.

Swelling study

The swelling study of the ENR/silica and ACM/silica hybrid composites was carried out in THF for 72 h under ambient condition. The equilibrium swelling index (α) was calculated from the following equation

$$\alpha = \left(\frac{w_f - w_i}{w_i}\right) \times 100 \tag{2}$$

where w_f and w_i are the final and the initial sample weights, respectively.

Dynamic mechanical thermal analysis (DMTA)

Dynamic mechanical thermal characteristics of the hybrid composite films were valuated in a DMTA IV (Rheometric Scientific) under tension mode. The experiments were carried out at a frequency of 1 Hz. The measurements were taken from −80 °C to 100 °C for ACM/silica and ENR/silica and 0 °C to 100 °C for PVA/silica hybrids at a heating rate of 2 °C/min. The data were analyzed using RSI Orchestrator application software on an ACER computer attached to the machine. The storage modulus and loss tangent (tan δ) were measured for all the samples under identical conditions.

Mechanical property analysis

The mechanical properties of the composites were evaluated with a universal testing machine (UTM, Zwick 1445) on tensile specimens, punched out from the cast films using ASTM Die C. The mechanical tests were carried out as per ASTM D 412-99 method at 25 ± 2 °C at a cross head speed of 500 mm/min. The average value of three tests is reported for each sample.

Results and discussion

Morphological investigations and optical clarity of the films

Figure 2 demonstrates the morphological observations of the polymer/silica hybrid composites in terms of TEM, SEM and EDX. Visual appearance of the representative composite films is also shown in the figure. OD, quantifying the clarity of the films is reported in Table 1. The TEM micrograph (Fig. 2a) of ACMp1 prepared at pH ~ 1.0–2.0 shows a combination of spherical silica particles (of average dimension 90 nm) and aggregated silica structures (average dimension of 300 nm) as dark portions in the figure. Homogeneous distributions along with few aggregated structures of silica are also evident from the EDX silicon mapping of ACMp1, shown in Fig. 2b. This figure actually illustrates the broader view of Fig. 2a as the former is taken at lower magnification compared to the later. Fig. 2c exhibits the SEM micrograph of ACMp5, prepared at pH ~ 5.0–6.0 which clearly displays aggregated silica structures where the average dimension of the aggregates is > 1 μm. The EDX study of the same sample in Fig. 2d further confirms the SEM observation, as it

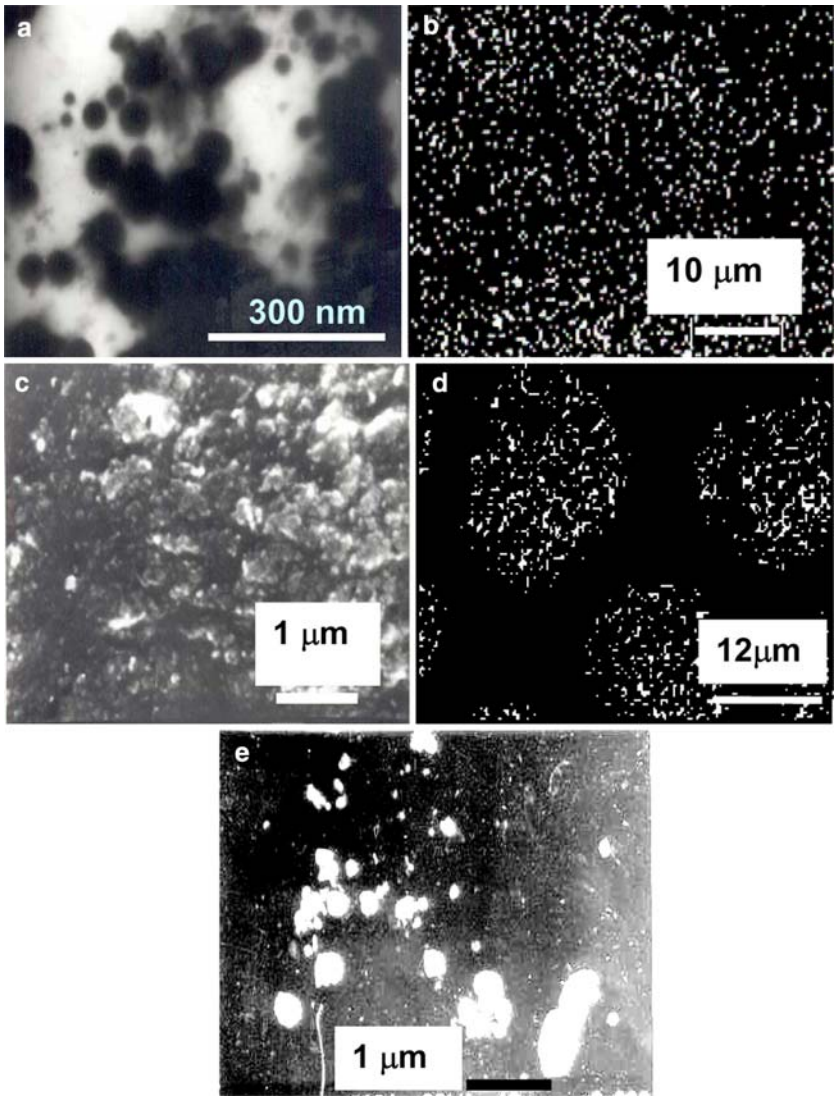

Fig. 2 Morphological observations of the hybrid composites: (**a**) TEM image of ACMp1; (**b**) EDX silicon mapping of ACMp1; (**c**) SEM micrograph of ACMp5; (**d**) EDX silicon mapping of ACMp5; (**e**) SEM micrograph of ACMp9; (**f**) TEM micrograph of ENRp1; (**g**) SEM image of ENRp5; (**h**) visual appearance of ENRp5 demonstrated over the logo with and without film (average thickness 0.25 mm); (**i**) SEM micrograph of ENRp9; (**j**) TEM micrograph of PVAp1; (**k**) SEM micrograph of PVAp9; (**l**) visual appearance of PVAp9 shown against the logo (average film thickness 0.25 mm) and (**m**) visual appearance of PVAp12 (average film thickness 0.25 mm)

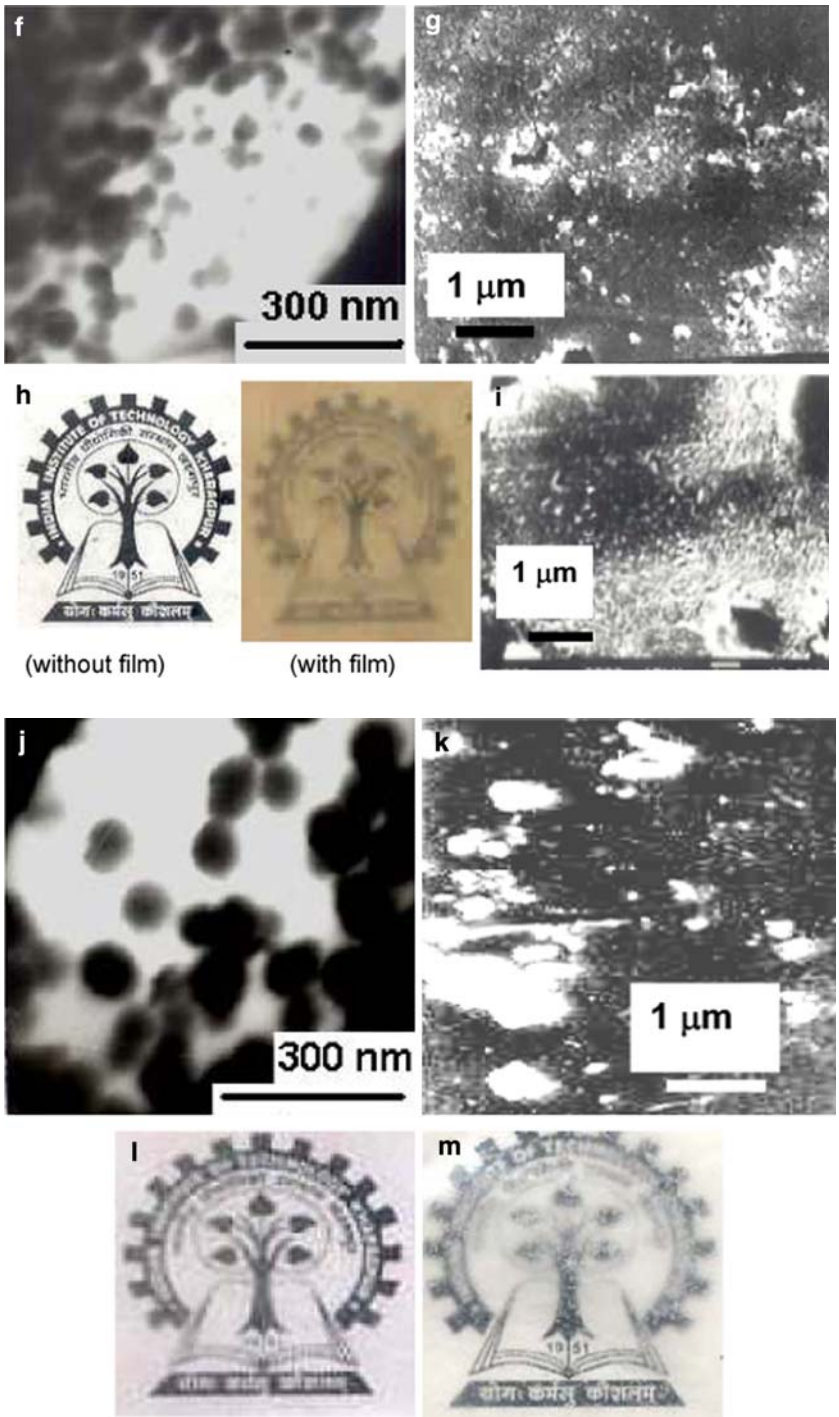

Fig. 2 continued

indicates local agglomeration of the silica phase within the hybrid composite. SEM picture for ACMp9 in Fig. 2e (at still higher pH) also demonstrates the agglomeration of the white inorganic phase within the rubber matrix and the dimension of the biggest cluster shown in the figure is about 1 μm. It indicates inhomogeneous distribution of inorganic phase It is clear that the silica particles tend to form aggregated structures in the hybrid composites beyond pH 2.0. It should be mentioned that the size of the silica particles increases with the increase in TEOS concentration due to higher amount of silica generation [13–15]. The infrared OD data in Table 1 quantifies the appearance of these hybrid composites. The OD increases about 540% for ACMp5 and 500% for ACMp9 with respect to ACMp1. It is principally due to micro-phase sepa-

ration at the organic–inorganic interface resulting from the agglomeration of silica particles.

Figure 2f depicts the TEM micrograph for ENRp1 hybrid composite prepared at pH ~ 1.0–2.0. The average dimension of the silica particles in ENRp1 (Fig. 2f) is about 75 nm. It is to be noted that the silica particles are more uniformly dispersed compared to that in ACMp1. The SEM micrograph for ENRp5 in Fig. 2g demonstrates the existence of aggregated silica particles along with some fine silica dispersion within the rubber matrix which may be due to the delayed catalytic effects on TEOS at higher pH (pH > 2.0). Visually a composite film of ENRp5 of average thickness 0.25 mm appears hazy, when it is placed over a logo, shown in Fig. 2h. The haziness may be caused on account of micro-phase separation that has taken place due to the formation of silica aggregates in ENRp5, which scatters light (further confirmed by 170% increment in OD from ENRp1 in Table 1). The SEM micrograph for ENRp9, shown in Fig. 2i, also demonstrates the aggregation of silica particles (OD is 300% higher than ENRp1, Table 1). However, the composite becomes completely opaque at still higher pH range (pH 12.0–13.0) evident from very high OD value (400% compared to ENRp1), reported in Table 1.

Figure 2j shows the TEM micrograph for PVAp1 where the average diameter of the spherical silica particles is around 90 nm (OD 0.08). Based on our previous investigations [15, 16], it has been known that with higher proportion of water, the silica particles tend to aggregate due to rapid hydrolytic reaction of TEOS under acidic conditions. In aqueous PVA, the silica particles are predominantly in nanodimensions, which is probably due to enhanced interfacial interaction between the organic and inorganic components. The SEM micrograph for PVAp9 in Fig. 2k illustrates that the silica particles are in aggregated form within the PVA matrix (average size of 2 μm). There are also some fine silica dispersions observed in the figure. The composite does not appear hazy, like similar compositions of other systems, when placed over the same logo shown earlier (the average film thickness was 0.25 mm, OD 0.10) in Fig. 2l. It is attributed to maximum concentration of hydroxyl groups (OH) in PVA which facilitate interaction with silica at the organic–inorganic interface compared to that of ENR and ACM systems. It may be mentioned here that the optical clarity of the neat ACM and neat ENR films (thickness 0.25 mm) is comparatively lower (OD values are 0.16 and 0.15, respectively) than that of PVA film of same thickness (OD is 0.06). But the aggregation of silica particles in PVA is enhanced when the pH is further increased (12.0–13.0), which is illustrated by the visual appearance of PVAp12 in Fig. 2m. The 0.25 mm thick film appears partially opaque against the logo (OD 0.15, 200% higher than PVAp1).

Infrared spectroscopic analysis

Figure 3a–c displays representative Fourier Transform infrared (FTIR) spectra for ACM/silica, ENR/silica and PVA/silica hybrid composites, respectively, prepared at different pH ranges. The spectrum for the neat polymer in each case is also included for comparison. The characteristic absorption peaks are reported in Table 2. Some of the peaks of the control polymer interfere with Si–O–Si stretching and silanol stretching absorptions. In ACM/silica, the symmetric ester alkyl group (C–O–C) of the polymer overlaps with the asymmetric Si–O–Si stretching and gives a peak at around 1020 cm^{-1}. Broad absorption due to asymmetric C–O stretch for epoxy in ENR also interferes with the hybrids in this region. For PVA/silica, sharp peak due to C–O stretching movements in PVA at 1040 cm^{-1} interferes with asymmetric Si–O–Si stretching and causes an about 20 cm^{-1} peak shift towards the higher value. In our previous communication we have already reported this peak shift [14]. On the other hand there is no significant peak shift for ACM/silica, while for ENR/silica, it would be erroneous to predict any shift due to the broad absorption pattern. The silanol absorption band at 920 cm^{-1} in PVA/silica interferes with C–O–C symmetric stretching for some ether linkages, possibly generated due to condensation of O–H groups on dissolution of PVA in boiling water. In ENR/silica, a small but sharp peak is obtained for silanol at 950 cm^{-1} and for ACM/silica, this absorption is relatively wider and appears in the similar region.

Figure 3d gives a comparative plot of the two important peak absorption areas, one due to Si–O–Si asymmetric stretching and the other for the silanol, which are compared with the constant peak absorbance at 1446 cm^{-1} (1420 cm^{-1} for PVA) due to C–H bending movements in the hybrid composites. These data points are obtained after de-convoluting the infrared spectra of the polymer/silica hybrid nanocomposites (Fig. 3a–c). The representative specimens shown in the plot demonstrate that composites prepared at lower pH (pH = 1.0–2.0) exhibit relatively higher absorption for silica and silanol (Fig. 3d). It is due to homogeneous dispersion of silica nanoparticles within the hybrid composites, as already seen under TEM. These silica nanoparticles may be composed of short-length silica chains and ring structures [17], which have fair amount of uncondensed silanol groups to interact with the binder polymer. At higher pH (pH > 2.0), the silica

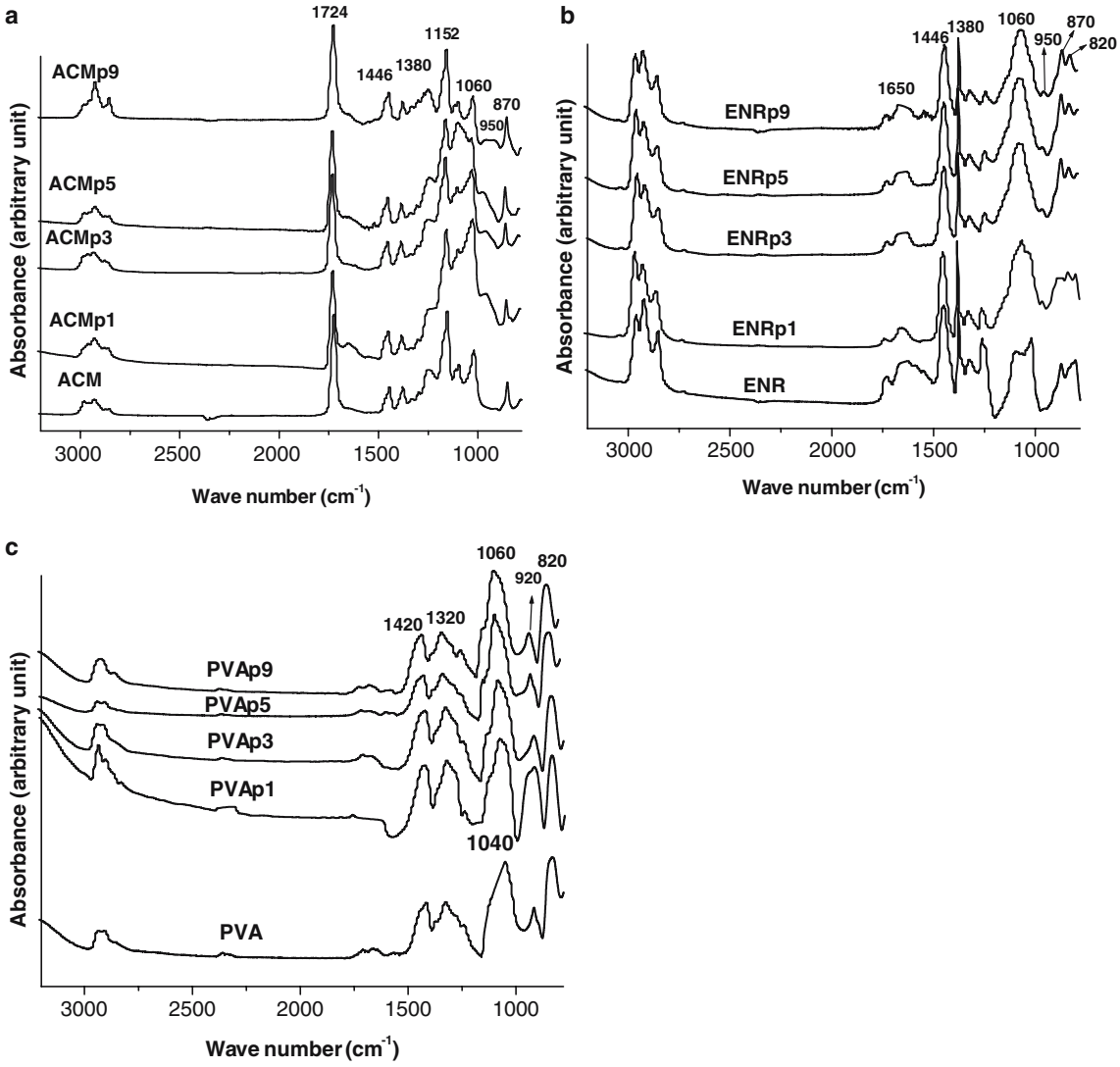

Fig. 3 FTIR spectra for (**a**) ACM/silica; (**b**) ENR/silica; and (**c**) PVA/silica hybrid composites; and (**d**) variation in peak intensity of silica and silanol with respect to C–H bending vibrations in representative hybrids

particles show predominant aggregation along with some fine dispersion (refer to the Fig. 2c, g, i and k) although the composites become in-homogeneous and lose transparency (Table 1). The finer silica particles have relatively higher concentration of silanol groups compared to aggregates as already mentioned. However, the ash content data of the hybrid composites, reported in Table 1, indicate that the extent of silica generation within the hybrid composites is nearly same at all the pH ranges. Therefore, variation of pH and also different functional groups in the binder polymer do not affect the silica generation but possibly delays the hydrolysis of TEOS at higher pH (pH > 2.0) and causes local silica aggregation.

The optimum pH for the generation of nanocomposites is observed in the range from 1.0–2.0. In this condition, the polymer-filler interaction is expected to be maximum. In ACM/silica, weak dipolar interaction exists at the organic–inorganic interface, as the hybrid composites prepared at different pH levels are completely soluble in THF under ambient condition. In ENR/silica, at low pH (pH = 1.0–2.0, ENRp1), the interactive force is the hydrogen bonding, formed between silanol and the OH groups of ENR (produced from the acid catalyzed ring opening reaction at the epoxy sites) whereas the same interaction is significantly lowered at higher pH (pH > 2.0). This is evident from the disappearance of the epoxy ring vibration peak at 870 cm^{-1} in ENRp1 (Fig. 3b) and gradual increase in equilibrium swelling index (α, in %) in THF for 72 h under ambient condition (α_{ENRp1} = 579, α_{ENRp5} = 665 and α_{ENRp9} = 1,090). Higher pH (pH > 2.0) probably

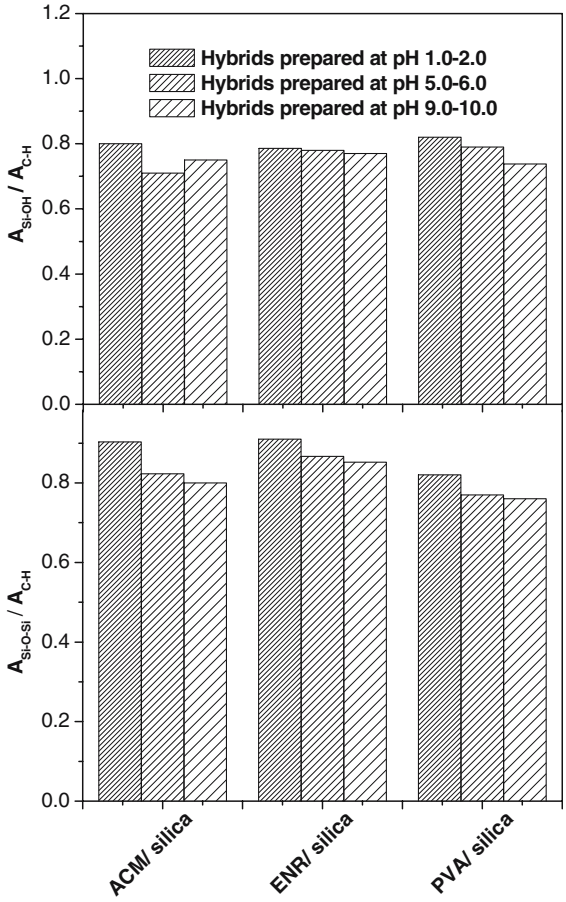

Fig. 3 continued

restricts the ring opening reaction at epoxy sites in ENR, which may be the reason for lower organic–inorganic interfacial interaction in ENRp3-p9. In PVAp1, stronger hydrogen bonding could be anticipated between PVA and silica compared to ENRp1, evident from broad absorption peak area due to silanol in Fig. 3c. Also the variation in swelling indices in PVA/silica hybrids (α_{PVAp1} = 185, α_{PVAp5} = 225 and α_{PVAp9} = 298, measured in water for 72 h at ambient condition) is much lower compared to the ENR/silica hybrids prepared at identical pH. Huge concentration of interactive OH groups on PVA molecule may be the reason for this observation. Following is the model that shows the probable molecular structure in ENRp1 and PVAp1. (Scheme 1)

In the model the inorganic moiety represents nanosilica particle with remnant silanol groups.

Dynamic mechanical thermal analysis

Figure 4 demonstrates the representative dynamic mechanical thermal analysis results for the polymer/silica hybrid composites in terms of storage modulus

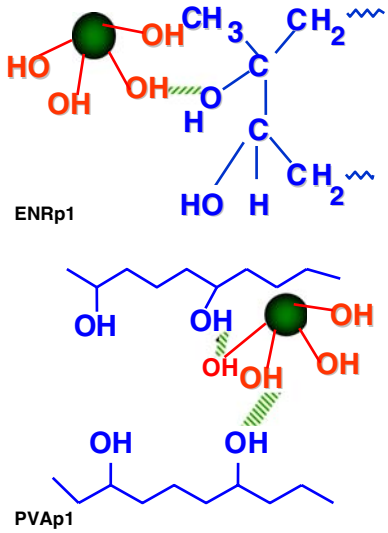

Scheme 1

(log scale) and loss tangent in the temperature range of −80–100 °C for ACM and ENR/silica hybrids and 0–100 °C for PVA/silica hybrids. For all the systems, the storage modulus of the neat polymer is lower than that of the hybrids in the whole temperature range on account of the silica fillers present within the matrix (Fig. 4a, b and c, respectively). But the level of difference in modulus between the control and the hybrids is purely a function of relative interaction between the organic and the inorganic phases and also its structure (whether the inorganic phase is finely dispersed or agglomerates). For the ACM/silica system, the modulus value is highest for ACMp1, as the size of silica particles are relatively smaller compared to other hybrids of same series, already depicted through microscopic study. However, at a temperature above 0 °C, the modulus of ACMp5 levels with ACMp1. This may be due to the fact that under sinusoidal stress

Table 2 Characteristic infrared absorption peaks for the polymer/silica hybrid composites

Peak value (cm^{-1})	Peak assignment
1,724	C=O stretching (ACM)
1,650	C=C stretching (ENR)
1,446 (1,420 for PVA)	C–H bending
1,380 (1,320 for PVA)	C–H deformation (for PVA)
1,152	Asymmetric C–O–C stretch (ester in ACM)
1,100–1,000	Asymmetric Si–O–Si stretching, C–O asymmetric stretching
950 (920 for PVA)	Si–OH stretching, symmetric C–O–C stretching (PVA)
870	C–O–C epoxy ring vibration
820	OH deformation (PVA), symmetric Si–O–Si stretching

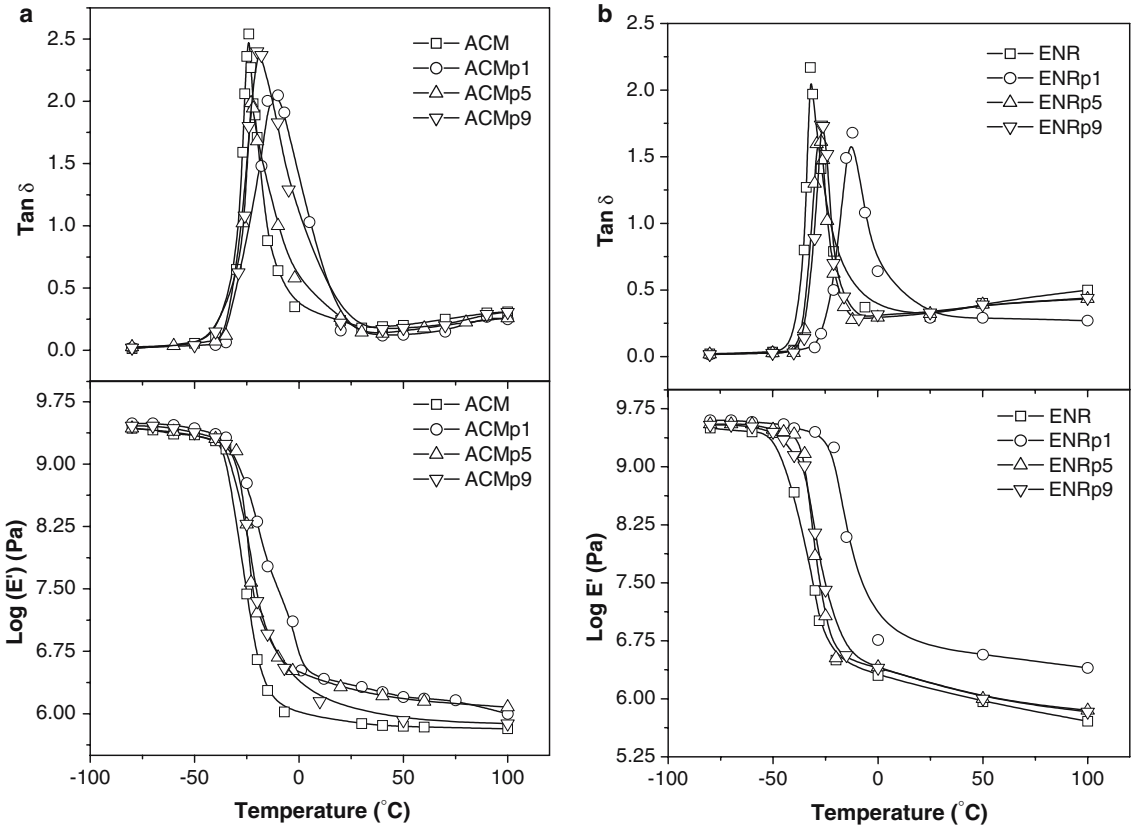

Fig. 4 (**a**) Storage modulus and tan δ plots for the representative ACM/silica hybrid composites. (**b**) Storage modulus and tan δ plots for the representative ENR/silica hybrid composites. (**c**) Storage modulus and tan δ plots for the representative PVA/silica hybrid composites. (**d**) Plot of RF (E/E_0) at different pH for the hybrid composites at the rubbery region (50 °C) in dynamic mechanical analysis

the relatively bigger silica clusters in ACMp5 may disintegrate to smaller size, which is responsible for the modulus comparable to that of ACMp1.On the other hand, ACMp9 shows the lowest modulus among all the ACM/silica hybrid systems (Fig. 4a). This result could be further demonstrated by considering the modulus values at the three different temperatures (−50 °C, *T*g and 50 °C) arbitrarily chosen, registered in Table 3. The difference in modulus values among the hybrids becomes more prominent especially in the rubbery region (above *T*g) compared to that in the glassy region (below *T*g).

ENRp1 shows the highest modulus in the ENR/silica hybrid composite series (Fig. 4b and Table 3) as anticipated from the morphological evidence. Unlike ACM/silica system, ENRp5 and ENRp9 exhibit almost similar modulus which is very close to that of the control polymer, especially at high temperature (Fig. 4b and Table 3). On the other hand, the difference in modulus between PVAp1 (which naturally registers highest modulus in the PVA series) and neat PVA is higher compared to ENR/silica system, observed from Fig. 4b and c. It may be due to the effect of enhanced interaction between the organic phase (PVA) and the inorganic phase (silica) within the composite. PVAp9 demonstrates lower modulus compared to PVAp5, especially beyond 25 °C, which may be due to aggregated structures of the filler that get detached from the polymer chains for their higher mobility at this temperature. This is further illustrated by the modulus values at three different temperatures (5 °C, *T*g and 50 °C) from Table 3. Fig. 4d illustrates the reinforcement factor (RF) (E'/E'_0) of the hybrid composites at different pH in the rubbery region (50 °C). PVA/silica is superior in the series, while mixed response is obtained from ENR/silica and ACM/silica systems though the modulus decreases with increasing the pH in all the cases. This observation is significant as it gives an insight into the comparative polymer filler interactions when the polymer chains are in mobile condition (at higher temperature). The superiority of PVA/silica hybrid is suggested due to higher interactive nature of PVA with silica compared to ENR and ACM in the entire pH range studied. However, higher is the interaction, larger is the change with variation of pH. Lowering of RF is due to the

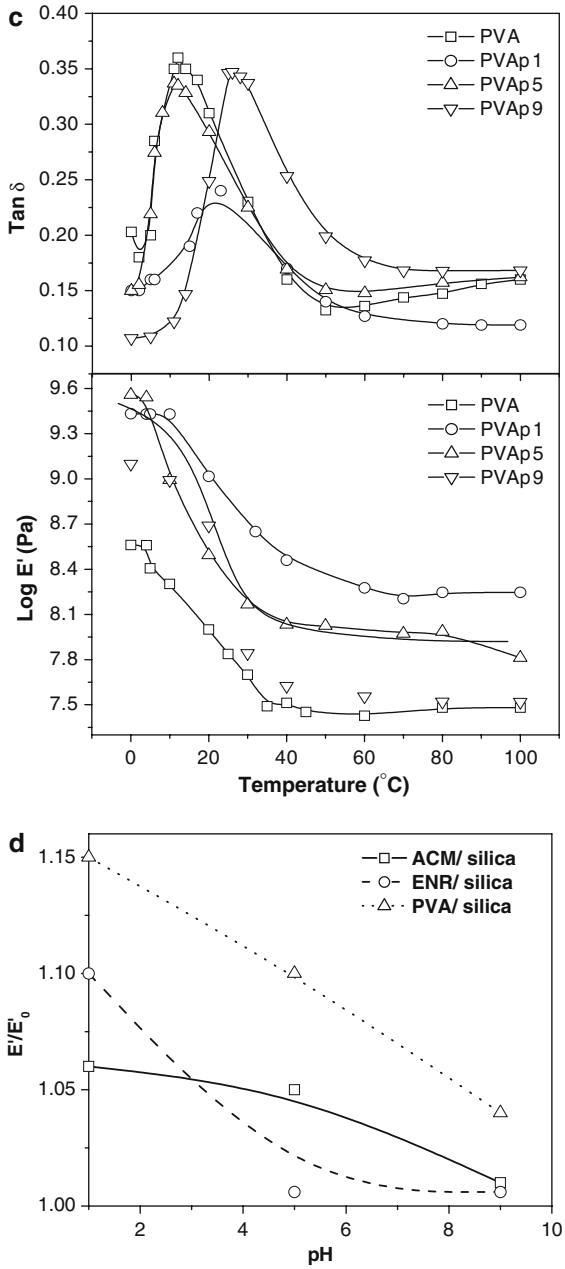

Fig. 4 continued

detachment of filler aggregates from the polymer surface. Also at higher pH, silica agglomeration is observed under a microscope. The higher value of ACMp5 compared to ENRp5 in the figure could be explained on the basis of disintegration of silica agglomerates and lower fall of $E'/E'0$ with respect to pH, as mentioned earlier. Under basic pH both ENRp9 and ACMp9 exhibit similar value.

ACMp1 and ACMp5 show almost similar tan δ_{max} in the tan δ versus temperature plot (Fig. 4a and Table 3) though for ACMp9, this value is comparatively higher and is more close to that of the neat ACM. The Tg (temperature corresponding to tan δ_{max}) of ACMp1 is distinctly higher (−10 °C) than the rest of the hybrids (−23 and −20 °C for ACMp5 and ACMp9, respectively) in the same series, which is possibly due to relatively smaller dimension of the silica phase with higher surface area in ACMp1, requiring relatively higher thermal energy to mobilize the polymer chains during glass transition.

In the ENR/silica series, ENRp1 exhibits lowest tan δ_{max} (Fig. 4b and Table 3) possibly due to higher polymer-filler interaction, as anticipated. ENRp5 and ENRp9 show comparatively higher tan δ_{max} (1.68 and 1.74, respectively, Table 3) which indicate that there are more free ENR chains resulting from lower interfacial interaction between the organic and the inorganic components due to silica aggregation in the respective composites enhancing the loss compared to ENRp1. More negative Tg (−27 °C, Table 3) for these composites (ENRp5 and ENRp9) than that of ENRp1 (−12 °C, Table 3) is also consequential to this factor.

The situation is little complicated in the loss tangent plots of PVA/silica system shown in Fig. 4c. There is a significant decrease in tan δ_{max} from PVA to PVAp1 along with the positive shift in Tg, which is in line with the earlier observation (Fig. 4c and Table 3), though the Tg value for PVAp9 is almost the same as that of PVAp1 (Table 3). It may be due to the inherent complexity within the polymer (PVA) as there is an extensive inter- and intra-molecular hydrogen bond formation within the matrix as well as with residual solvent (water) and ethanol (by product of hydrolysis of TEOS). It has been confirmed by checking the repeatability of the result. Predominant polymer-filler interaction due to nanolevel dispersion of silica in PVAp1 compared to PVAp9, where the silica is in more aggregated form, reduces tan δ_{max} (Fig. 3c and Table 3) and restricts inter-chain movements in the former. This effect is already demonstrated through morphological study and the lower modulus values in the both glassy and rubbery regions.

Mechanical properties

The tensile stress–strain curves for the representative polymer/silica hybrid composites are shown in Fig. 5. ACM and ENR hybrid systems show yielding behavior when the samples are stretched beyond 300% (Fig. 5a and b, respectively) due to the uncured nature of the rubber matrix and also due to dewetting action of the filler at high extension within the hybrids. All the rubber/silica hybrids show high elongation (> 900%); however, the PVA/silica composites fail much early (Table 4). The breaking elongation especially of the

Table 3 Storage modulus and loss tangent values at three temperatures and *Tg* of the representative polymer/silica hybrid composites

Composite designation	Log E′ (Pa)			Tan δ			*Tg* (°C)
	Low temperature[a]	*Tg*	50 °C	Low temperature[a]	*Tg*	50 °C	
ACM	9.35	7.25	5.85	0.05	2.54	0.20	−24
ACMp1	9.43	7.70	6.20	0.04	2.04	0.12	−10
ACMp5	9.36	7.57	6.18	0.04	1.99	0.14	−23
ACMp9	9.38	7.35	5.92	0.04	2.40	0.18	−20
ENR	9.44	7.50	5.96	0.03	2.17	0.40	−32
ENRp1	9.50	7.80	6.57	0.03	1.61	0.29	−12
ENRp5	9.48	7.55	6.00	0.02	1.68	0.39	−27
ENRp9	9.45	7.60	6.00	0.02	1.74	0.39	−27
PVA	8.40	8.20	7.30	0.20	0.36	0.13	12
PVAp1	9.43	8.99	8.40	0.16	0.24	0.14	23
PVAp5	9.30	8.60	8.02	0.27	0.33	0.15	12
PVAp9	9.10	8.40	7.60	0.10	0.35	0.19	24

[a]For ACM and ENR, the data at −50 °C are included, while the values for PVA correspond to those at 5 °C

rubber/silica hybrid composites could not be recorded due to the limitations of the machine and therefore, the strength of the composites is taken as the maximum stress point in the stress–strain curve, exhibited in Fig. 5. For ACM/silica system, the strength of the composite prepared at lower pH (< 2.0) is highest. This, however, decreases with increasing pH of the medium beyond 2.0. The stress–strain curve for ACMp5 is almost similar to ACMp9, as evident from Fig. 5a. The strength of the composites is registered in Table 4. ACMp1 shows almost 300% improvement in strength compared to the controlled sample, while the improvement is 200% for ACMp5 and ACMp9. A similar trend is observed with the ENR/silica hybrid systems (Fig. 5b), though there is only 13% drop in strength from ENRp1 to ENRp3. This value is lower than that of the ACM systems prepared under the same condition. It may be pointed out that the initial strength of ENR is much higher than the ACM system. Also, there is more interactive organic–inorganic interface in ENR compared to ACM as investigated earlier [13, 14]. The stress–strain curves for PVA/silica hybrid composites are shown in Fig. 5c. All the composites elucidate predominant plasticization effect due to high humidity in the ambient air. This has been understood from higher strength (33 MPa) and modulus of the neat PVA sample (and lower elongation at break values) after annealing in an oven at 70 °C for 3 days as compared to that of the current values of the same sample**.** Neat PVA, PVAp5 and PVAp9 exhibit almost similar strength as evident from the figure, which is considerably lower than that of PVAp1. This is probably due to the inhomogeneous distribution of silica within the PVA matrix beyond pH 2.0 (refer to Fig. 2l and m). It should be mentioned that, although PVAp9 and PVAp1 possess almost similar *Tg* but the mechanical strength of the former is considerably lower than the later. Maximum strength is displayed by PVAp1, while PVAp3 shows comparatively lower strength (around 28%). Fig. 5d compares the %change in modulus $[(E - E_0) \times 100]$ against the pH of the reaction medium for the hybrid composites. The modulus values have been calculated from the slope of the initial linear portion of the stress–strain curves. The range of $[(E - E_0) \times 100]$ values in PVA/silica system is substantially higher compared to ENR/silica and ACM/silica; therefore, the PVA/silica hybrid composites are plotted separately in the figure. Existence of weakest interaction is clearly demonstrated between the organic and the inorganic phases in ACM/silica system (Fig. 5d), as the improvement in modulus for ACMp1 is the lowest compared to ENRp1 and PVAp1 (the value is appreciably higher for PVAp1). It is

Table 4 Mechanical properties data for the representative polymer/silica hybrid composites

Composite designation	Maximum tensile stress (MPa)	Tensile modulus[a] (MPa)	EB%
ACM	0.30	0.25	>900
ACMp1	1.30	0.30	>900
ACMp3	0.95	0.25	>900
ACMp5	0.90	0.25	>900
ACMp9	0.90	0.20	>900
ENR	2.00	0.55	>900
ENRp1	5.50	1.20	>900
ENRp3	4.80	1.10	>900
ENRp5	3.10	0.99	>900
ENRp9	3.05	0.99	>900
PVA	21.00	8.23	180
PVAp1	42.53	24.00	70
PVAp3	31.00	17.31	84
PVAp5	22.00	10.00	150
PVAp9	21.00	9.00	120

[a]The modulus values are calculated from the slope of the initial linear portion of the stress–strain curves

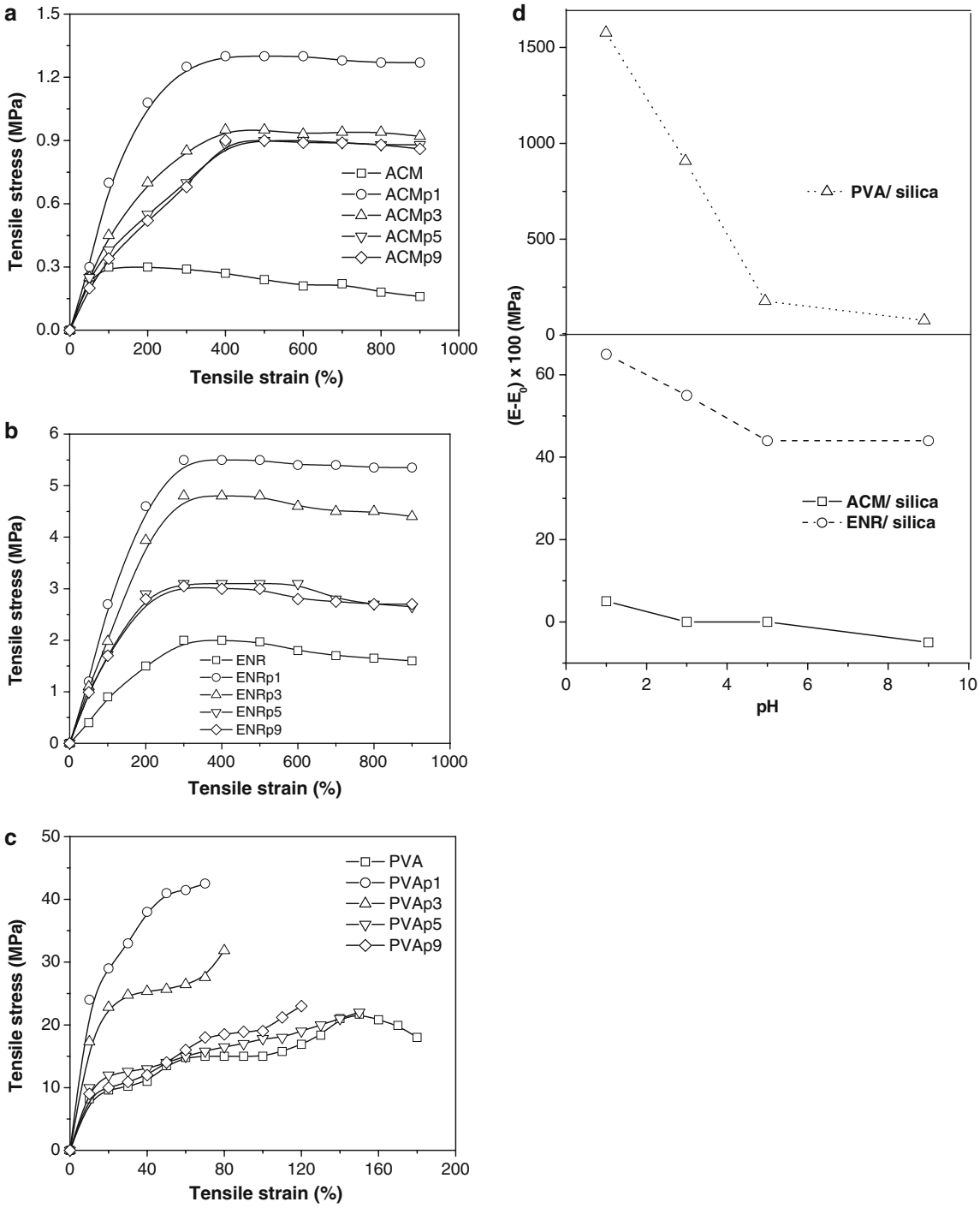

Fig. 5 (**a**) Tensile stress–strain curves for the representative ACM/silica hybrid composites. (**b**) Tensile stress–strain curves for the representative ENR/silica hybrid composites. (**c**) Tensile stress–strain curves for the representative PVA/silica hybrid composites. (**d**) Plot of % change in modulus for the hybrid composites, calculated from the slope of initial linear portion of the stress–strain curves in Fig. 5(**a**)–(**c**) against different pH level

attributed to gradual decrease in interactive sites over the respective polymers (PVA, ENR and ACM) within the nanocomposites. Moreover, ACMp3 and ACMp5 practically do not show any improvement (Fig. 5d), while ACMp9 gives a downfall of 5%, which is the outcome of silica aggregation and also due to de-wetting of the rubber, as mentioned earlier. All the systems elucidate the drop in tensile modulus on

increasing the pH which corroborates the earlier results of RF with variation in pH, described in the previous section. The decrease in tensile modulus is due to larger silica domains (> 1 μm) compared to the nano-silica particles (< 100 nm) which provides higher surface area for interaction with the polymer. The drop in modulus is much sharper for PVA/silica system (Fig. 5d) though, the respective values are distinctly higher than the ENR/silica and the ACM/silica systems at all pH. The sharp drop in PVA/silica hybrids may be due to predominant polymer–polymer interaction as a consequence of agglomeration of silica under high pH. This result delineates the importance of interactive organic–inorganic interfaces within the composites in order to improve the strength of the assembly.

Conclusions

ACM/silica, ENR/silica and PVA/silica hybrid composites have been prepared by sol-gel technique at 45 wt% TEOS at different pH levels. The structure and mechanical properties of the resultant composites have been measured and the following observations are made.

1. Morphology as investigated by TEM, SEM and EDX demonstrates the presence of stable nano-silica structures in the hybrid composites at lower pH (pH ≤ 2.0). At higher pH, the silica particles aggregate, which is probably due to slower catalytic effect on TEOS affecting the growth of silica within the polymer matrix. The extent of total silica generation is not affected by increasing the pH. All the nanocomposites visually appear transparent (display low infrared OD), while the composites containing aggregated silica structures are translucent to opaque (relatively higher OD values). Relatively stronger polymer-filler interaction at almost similar silica concentration in ENRp1 and PVAp1 compared to ACMp1 is anticipated from FTIR and solubility studies.
2. Dynamic mechanical study exhibits mechanical reinforcement in the nanocomposites, while for micro-composites formed at higher pH the effect is comparatively low due to the low surface area for interaction with the silica filler. There is about 10% drop of the ratio E/E_0 for the PVA/silica system in the rubbery region (50 °C), when the pH level is increased from 2.0 to 9.0. For the ENR/silica and ACM/silica, the same value is 9% and 5%, respectively. The nanocomposites (ACMp1, ENRp1 and PVAp1) show lowest tan δ_{max} value and the Tg shifts to higher temperature compared to the micro-composites on increasing the pH. PVAp9 shows almost similar Tg to that of PVAp1, which is due to various hydrogen bonded interactions with smaller molecules.
3. The tensile strength of the hybrid composite decreases with the increase in pH predominantly due to poor interfacial interaction and larger silica aggregates, although all the rubber/silica samples exhibit yielding and very high elongation (> 900%) on account of uncured nature of the matrix. A maximum of 100% drop in strength is observed for PVA/silica hybrid when the pH is increased from 2.0 to 9.0. ENR/silica and ACM/silica show a drop of 80% and 40%, respectively under identical conditions. At low pH (< 2.0), PVA/silica demonstrates highest improvement in tensile modulus compared to ENR/silica and ACM/silica. On increasing the pH, it decreases for all the systems (PVA/silica records sharpest decrease) principally due to poorer polymer-filler interaction resulting from the aggregation of silica.

References

1. Foussaier O, Menetrier M, Videau J-J, Duguet E (2000) Mater Lett 42:305
2. Hu ZM, Slaterbeck AF, Selisker CJ, Ridgway TH, Heinman WR (1999) Langmuir 15:767
3. Grady BP, Start PR, Mauritz KA (2001) J Polym Sci Part B: Polym Phys 39:197
4. Tang M-Y, Mark JE (1984) Macromolecules 17:2613
5. Jitianu A, Gartner M, Zaharescu M, Cristea D, Manea E (2003) Mat Sci Eng C23:301
6. Chan C-K, Peng S-L, Chu I-M, Ni S-C (2001) Polymer 42:4189
7. Chan C-K, Chu I-M (2001) Polymer 42:6823
8. Landry CJT, Coltrain BK, Brady BK (1992) Polymer 33:1486
9. Huang H-H, Orler B, Wilkis GL (1987) Macromolecules 20:1322
10. Zerda TW, Artaki I, Jonas J (1986) J Non Cryst Solids 81:365
11. Himmel B, Gerber T, Burger H (1987) J Non Cryst Solids 91:1322
12. Bandyopadhyay A, Bhowmick AK, De Sarkar M (2004) J Appl Polym Sci 93:2579
13. Bandyopadhyay A, De Sarkar M, Bhowmick AK (2004) Rubber Chem Technol 77:830
14. Bandyopadhyay A, De Sarkar M, Bhowmick AK (2005) J Mater Sci 40:5233
15. Bandyopadhyay A, De Sarkar M, Bhowmick AK (2005) J Appl Polym Sci 95:1418
16. Bandyopadhyay A, De Sarkar M, Bhowmick AK (2005) J Mater Sci 40:52
17. Socrates G (1980) In: IR characteristic group frequencies, Wiley, New York
18. Nishino H, Takahashi R, Sato S, Sodesawa T (2004) J Non Cryst Solids 333:284